Received: 20 January 2022 | Revised: 13 June 2022 | Accepted: 11 July 2022

DOI: 10.1111/jeb.14094

JOURNAL OF Evolutionary Biology eseb

RESEARCH ARTICLE

Inferring the demographic history of the North American firefly *Photinus pyralis*

Ana Catalan[1] | Sebastian Höhna[2,3] | Sarah E. Lower[4] | Pablo Duchen[5]

[1]Division of Evolutionary Biology, Ludwig-Maximilians-Universität München, Planegg-Martinsried, Germany

[2]GeoBio-Center, Ludwig-Maximilians-Universität München, Munich, Germany

[3]Department of Earth and Environmental Sciences, Paleontology & Geobiology, Ludwig-Maximilians-Universität München, Munich, Germany

[4]Department of Biology, Bucknell University, Lewisburg, PA, USA

[5]Institute for Organismal and Molecular Evolutionary Biology, Johannes Gutenberg University of Mainz, Mainz, Germany

Correspondence
Ana Catalan, Division of Evolutionary Biology, Ludwig-Maximilians-Universität München, Grosshaderner Straße 2, Planegg-Martinsried 82152, Germany.
Email: ana.catalan@gmail.com

Funding information
Deutsche Forschungsgemeinschaft, Grant/Award Number: 447192820, CA2207/3-1, HO6201/1-1 and HO6201/2-1

Abstract

The firefly *Photinus pyralis* inhabits a wide range of latitudinal and ecological niches, with populations living from temperate to tropical habitats. Despite its broad distribution, its demographic history is unknown. In this study, we modelled and inferred different demographic scenarios for North American populations of *P. pyralis*, which were collected from Texas to New Jersey. We used a combination of *ABC* techniques (for multi-population/colonization analyses) and likelihood inference (*dadi*, *StairwayPlot2*, PoMo) for single-population demographic inference, which proved useful with our RAD data. We uncovered that the most ancestral North American population lays in Texas, which further colonized the Central region of the US and more recently the North Eastern coast. Our study confidently rejects a demographic scenario where the North Eastern populations colonized more southern populations until reaching Texas. To estimate the age of divergence between of *P. pyralis*, which provides deeper insights into the history of the entire species, we assembled a multi-locus phylogenetic data covering the genus *Photinus*. We uncovered that the phylogenetic node leading to *P. pyralis* lies at the end of the Miocene. Importantly, modelling the demographic history of North American *P. pyralis* serves as a null model of nucleotide diversity patterns in a widespread native insect species, which will serve in future studies for the detection of adaptation events in this firefly species, as well as a comparison for future studies of other North American insect taxa.

KEYWORDS
ABC, demography, fireflies, node calibration, nucleotide diversity, population genetics

1 | BACKGROUND

The current distribution of a species is the result of an intricate evolutionary interplay of demographic processes and selection across natural populations. Deciphering the demographic history is the first approach to gaining an understanding towards why and how a species obtained its current distribution. The demographic history of a species is marked by a number of past and present events, such as geological activity (e.g. the formation of land bridges or mountain ranges), ice ages (e.g. the change in ice sheet area across the globe), glacial refugia (Hewitt, 2004) and, more recently, the active migration of populations into novel habitats (Mann, 2007; Roy & Lachniet, 2010). For North American taxa, there are several studies tackling the demographic history of various species of vertebrates and plants (Cione et al., 2015; Soltis et al., 2006). However, for insects, there are only a few studies investigating their demographic history,

and in most cases, the investigation is focused on economically important or invasive species (Arias et al., 2019; Havill et al., 2016), but see also (Hyseni & Garrick, 2019). Studies involving insect pests and invasive species provide important information on the demographic dynamics of such species, especially on their rapid colonization capability. Nevertheless, when studying native species to a particular ecosystem, we gain knowledge about how natural events such as geographic barriers, past temperature fluctuations and, more recently, anthropogenic activity shaped their demographic history.

The river basins (Mississippi, Tombigbee and Appalachiola rivers) and the Appalachian mountains have been reported to produce biogeographical breaks between species distributions (Myers et al., 2020; Soltis et al., 2006). How these or other barriers hinder insect distribution is ongoing research, with only a few examples hinting that the biogeographical barriers described in vertebrates and plants might not apply to insects (Hyseni & Garrick, 2019; Jaskuła et al., 2021; Lait & Hebert, 2018).

In this study, we gained insight into natural insect colonization patterns in North America by modelling the population history of the firefly *Photinus pyralis*. Fireflies (Coleoptera: Lampyridae) are a diverse group of conspicuous beetles that produce bioluminescence as an aposematic signal against predators (Cock & Matthysen 1999), to lure prey (Lloyd, 1975) and to attract potential mates (Lewis & Cratsley, 2008). Of the over 2000 described firefly species, *P. pyralis* has a particularly well-documented and wide geographical distribution, with collections from Ontario, Canada (Fallon et al., 2018), to Venezuela in South America (The Bavarian State Collection of Zoology, www.zsm.mwn.de) (Figure S1). The ample geographic distribution of *P. pyralis* offers us the opportunity to investigate the migration routes taken by natural insect populations and start exploring the demographic events that lead to the distribution pattern that we observe today.

In the present study, we investigated the demographic history of North American *P. pyralis* through demographic modelling of single nucleotide polymorphisms (SNPs) derived from double digest Restriction-site Association DNA sequencing (ddRADseq) data from 12 populations. The sampling of *P. pyralis*, from Texas to New Jersey, covers its complete distribution in North America. Previous work with this data revealed population structure among these populations as well as heterogeneous levels of nucleotide diversity and genetic distances across populations (Lower et al., 2018), suggesting a complex demographic history among populations. Nevertheless, a demographic inference analysis is missing for this species. Beside the genetic diversity found across populations, phenotypic traits such as life cycle length (Fallon et al., 2018), flash colour (male light emission peak wavelength) (Sander & Hall, 2015) and body size (Vencl & Carksib, 1998) have been described and hypothesized as polymorphic traits across *P. pyralis* populations. Whether this variation is due to adaptation, genetic drift and/or demography is still to be elucidated.

By using population-level RADseq data and by generating population genetic summary statistics, we proposed and tested various demographic scenarios for *P. pyralis*. Additionally, we generated a dated phylogeny in order to estimate the age of the node leading to *P. pyralis*, an estimate that informs us on the approximate maximum age of the most ancestral population of this species, beyond the presently studied populations. With this work, we generated the first hypotheses regarding the demographic history of North American populations of *P. pyralis* and include an estimate of the age of the most ancestral population of this species. Furthermore, characterizing the nucleotide diversity patterns left by demography alone sets the base to detect nucleotide patterns that deviate from neutral expectations.

2 | METHODS

2.1 | Clustering for demographic modelling

The data of this study consist of 2019 single nucleotide polymorphisms (SNPs) extracted from ddRAD sequencing data from 15 individuals from each of 12 populations of *P. pyralis* from North America (Table S1), as described in Lower et al., 2018. Following the population genetic analysis presented in Lower et al., 2018, the geographical location of the sampled populations and our hypotheses of possible colonization scenarios, we propose three population categories: Texan (shown in grey), Central (blue) and Eastern (light blue) (Table S1, Figure 1). Pooling the populations in three linages allows us to test for fewer and more streamlined demographic scenarios. To test for genetic congruence of these three clusters, we quantified the probability that the different populations were assigned to one of the clusters, using a discriminant analysis of principal components (DAPC) (Jombart et al., 2010), as implemented in the R package *adegenet* (v1.4.2) (Jombart & Ahmed, 2011). For the DAPC analysis, we kept three PCs and three discriminant functions. We also explored the pooling in three clusters by using fastSTRUCTURE (Raj et al., 2014) with $k = 3$. Raw ddRAD data are available in the NCBI Short Read Archive (SRA) repository: Accession SRP157802. VCFs used in the study can be found at Figshare: DOI https://doi.org/10.6084/m9.figshare.5771979 (Lower et al., 2018).

2.2 | Demographic analyses using approximate Bayesian computation (ABC)

We took two independent approaches to infer the possible colonization pathways between the Eastern, Central and Texan cluster : (1) we pooled the populations within each geographical category (Table S1), and (2) we took one random population from each cluster. For the second approach, we repeated the sampling three times, each with a different combination of individual populations. The populations sampled were DETX, VATX, DEMI, BYMS, SLMO, MANJ, ATGA and HFTN. The random population combinations are DETX-DEMI-MANJ, VATX-BYMS-ATGA and VATX-SLMO-HFTN. By taking these two approaches, we aimed at identifying if the most-probable colonization pathway is supported by both the pooled- and/or single-population combinations (Papadopoulou & Knowles, 2015).

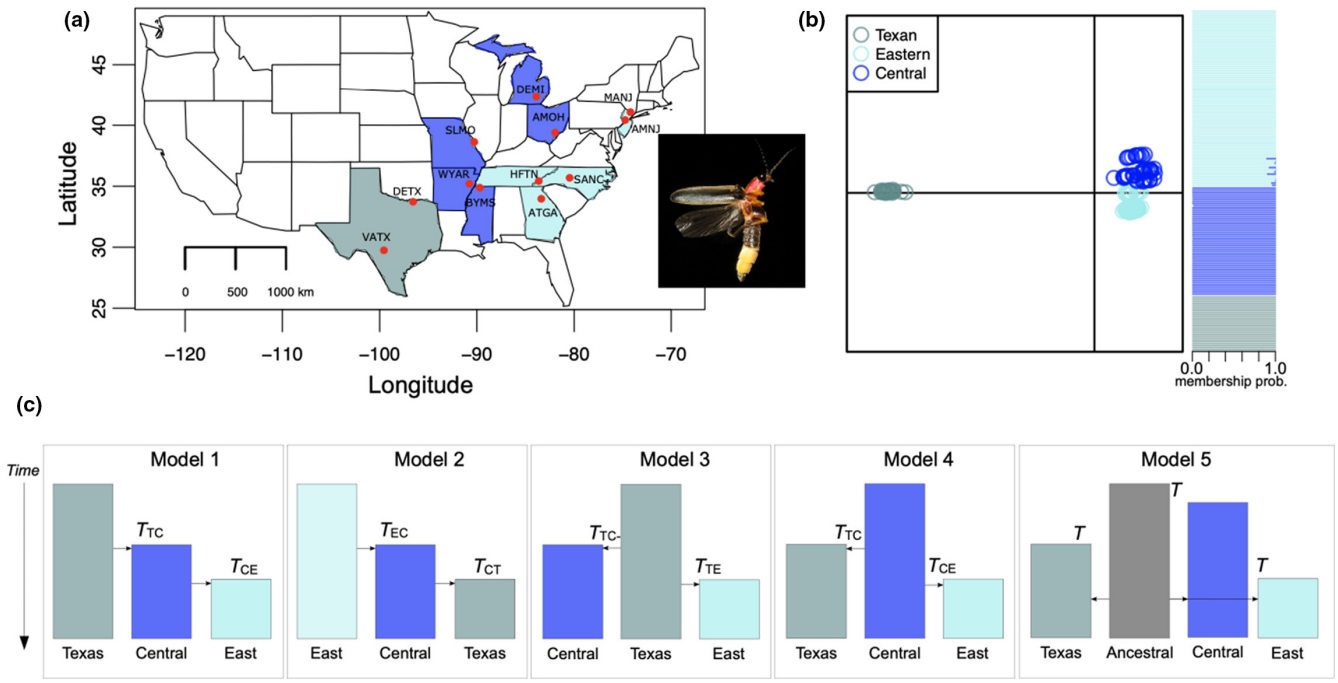

FIGURE 1 (a) Map of the United States showing the sampled populations of *P. pyralis* (red dots; adapted from Lower et al., 2018). The y-axis shows the latitude (N°), and the x-axis shows the longitude (W°). The three colours represent the three population clusters used in this study. Grey: Texan population, blue: Central population, and light blue: Eastern population. Inset: *Photinus pyralis*, credit: Creative Commons. (b) Genetic clustering of all sampled individuals into three distinct genetic clusters defined by a discriminant analysis of principal components (DAPC), including cluster probabilities. Each dot represents a single individual (Texas: $N = 25$, central = 49, eastern = 80; Total: 154). (c) Demographic history models tested for *P. pyralis*. Boxes represent effective populations sizes (*Ne*) of each population. T_{CE}: split time between the Central and Eastern populations, T_{TC}: split time between the Texan and Central populations. *T*: split time from a single putative ancestral population. All population sizes are estimated with respect to Ne_{Texas}, therefore $Ne_{Texas} = 1$. Population labels: AMNJ: Amwell, New Jersey; AMOH: Amesville, Ohio; ATGA: Athens, Georgia; BYMS: Byhalia, Mississippi; DEMI: Dexter, Michigan; DETX: Denison, Texas; HFTN: Hickory Flats Branch, Tennessee; MANJ: Mahwah, New Jersey; SANC: Salisbury, North Carolina; SLMO: St. Louis, Missouri; VATX: Vanderpool, Texas; WYAR: Wynne, Arizona

We tested the following multi-population demographic models. *Model 1*: The Texan population as the ancestral population, with subsequent sequential colonization of the Central and Eastern populations. *Model 2*: The Eastern population as the ancestral population, with subsequent sequential colonization of the Central and Texan populations. *Model 3*: The Texan as the ancestral population, with independent colonization of the Central and Eastern populations. *Model 4*: The Central population as the ancestral population, with independent colonization of the Texan and Eastern populations. *Model 5*: Non-sequential colonization of the Texan, Central and Eastern populations from a putative singl ancestral population (Figure 1c).

2.3 | Data preparation for demographic analyses

We are aware that, ideally, a demographic analysis benefits the most from neutral sites, where selection does not confound the effects of demography, and where the maximum number of polarized SNPs are available (the more data, the more power to infer demographic parameters, Excoffier et al., 2013). Given our data, we took the following steps to ensure an unbiased demographic analysis: (1) From the original set of 2019 SNPs, we discarded all singletons, or class '1' of the site-frequency spectrum (SFS). Low-frequency variants are more sensitive to filtering pipelines, yielding a lower mapping quality for the singleton class (Duchen et al., 2013). (2) Because there is no outgroup sequence, we summarized the data in statistics that are unaffected by polarization (see below). In our case, this implies that excluding singletons means that we also excluded class '*n*-1' from the SFS. (3) Even though our SNP dataset consists of filtered variants after F_{st} outlier analysis, we performed additional simulations to account for selection as an evolutionary force that might have helped maintain a proportion of the variants present in our data and which could not be filtered out by the F_{st} outlier analysis (see 'ABC simulations').

2.4 | Observed summary statistics

From the observed data, we calculated the following summary statistics: number of segregating sites *S*, Watterson's θ_W (Watterson, 1975), π and distance of Nei and Li (1979), Tajima's *D* (Tajima, 1989), linkage disequilibrium Z_{nS} (Kelly, 1997), the folded SFS, Weir-Cockerham's F_{st} (Weir & Cockerham, 1984) and the Wakeley–Hey 'W' summaries of the joint folded SFS (Wakeley & Hey, 1997). As explained before, all

the above-mentioned statistics are unaffected by the polarization of the observed SNPs. Here, statistics S, θ_W and π summarize nucleotide diversity, Tajima's D and W summarize the SFS, Z_{nS} summarizes linkage disequilibrium, and the distance of Ne_i and F_{st} describes population differentiation. Furthermore, simulations were done to recreate the variant-generation process of our RADseq data.

2.5 | Simulations

To recreate the variant-generation process of our RADseq data, we simulated exactly 2019 SNPs (for 308 chromosomes: 50, 126 and 132 chromosomes representing the Texan, Central and Eastern populations, respectively), for each of the four demographic models described in Figure 1c (see Section 3 for a description of each model). These coalescent simulations were done with the program *msms* (Ewing & Hermisson, 2010) using command lines of the form:*msms-ms 308 50000 -s 2019 -I 3 50 126 132 -n 2 tbs -n 3 tbs -ej tbs 3 2 -ej tbs 2 1 -SAa tbs*. This command tells *msms* to perform 50 000 simulations, each with 308 chromosomes (50, 126 and 132 chromosomes for each population), 2019 SNPs, population sizes (relative to population 1) determined by -n 2 and -n 3, and colonization events in the ordered indicated by the flags *-ej*. The term *tbs* stands for 'to be specified', which means that it is read from an external file. For instance, *−ej tbs 3 2* means that population 3 joins population 2 (backwards in time) at time *tbs*, which will be read from a file with prior values for this parameter. Similar command lines (where the colonization order differs) were used for the different demographic models.

To exactly recreate the treatment given to the observed data (see Section 2.3) from the simulated sites, we removed the SFS classes '1' (singletons) and 'n-1' for each population, and calculated all summary statistics described above. Recall that these summary statistics do not depend on the polarization of the data, that is their values are the same whether we know which alleles are ancestral or which ones are derived. Given that the observed SNPs coming from RAD sequencing are spread throughout the genome (including both conserved and neutral regions), we expect that some degree of selection has helped maintain that diversity for many of those sites. For this reason, we included the *msms* switch *-SAa* with a value of selection drawn from a prior distribution. We repeated the simulation procedure 50 000 times for each demographic model.

2.6 | Model choice using ABC

To estimate confidence in the estimated models (please refer to the results section for model description), we used Approximate Bayesian Computation (ABC), with 50 000 simulations per model to calculate the posterior probabilities of each of the four demographic scenarios using the R package *abc* (Csilléry et al., 2012). Model choice was based on the following summary statistics: θ_W, π, Tajima's D, Z_{nS}, W statistics, distance of Nei and *Fst* (we did not use the number of segregating sites S because it is directly correlated with θ_W, or the folded SFS because it is well summarized with the W statistics and Tajima's D). We validated the power (I − type_II_error) of the model-choice procedure by sampling a random vector of 'pseudo-observed' summary statistics from the simulations and re-calculating the probability of them coming from one of the four models. We performed this validation 100 times and scored the number of times the right model was chosen. Next, we performed model choice for the observed vector of summary statistics. Finally, to check how well the best model can predict the observed data, we plotted the distributions of summary statistics under the best model against the corresponding observed statistics.

2.7 | Parameter estimation

Parameter estimation was accomplished by using both the rejection (Pritchard et al., 1999; Tavare et al., 1997) and regression (Beaumont et al., 2002) algorithms using the R package *abc*. Briefly, we kept ('as accepted') the closest simulations to the observed summary statistics and generated distributions of their associated parameters. These distributions represented an approximation of the posterior probability of each particular parameter based on the 'rejection' algorithm (Pritchard et al., 1999; Tavare et al., 1997). Then, by performing a local regression between the accepted simulations and their corresponding parameters, an improved version of this posterior probability can be generated (Beaumont et al., 2002). To reduce the high dimensionality of the summary statistics while keeping the maximum amount of information still available, we used partial least squares (pls) in an ABC context (Wegmann et al., 2009). The ABC regression step for parameter estimation was performed with the pls-transformed statistics. A validation of parameter estimation was also performed by using the pseudo-observed statistics from the simulations and re-estimating the parameters with the regression algorithm.

2.8 | Demographic inference of single populations

To further investigate the demographic history of *P. pyralis*, we also analysed our data using *dadi* (Gutenkunst et al., 2009) and *StairwayPlot2* (Liu & Fu, 2020). First, we used *dadi* and fitted five different commonly used single-population models: (1) neutral equilibrium model: this is the null model and assumes a constant population size. (2) Two-epoch model: this model describes one population-size change that could either be a decrease or an increase. (3) Growth model: this one describes an exponential population-size change reflecting exponential growth or decline. (4) Bottle-growth model: this model describes a bottleneck (or expansion) event followed by a population growth/decline. (5) Three-epoch model: this model describes two population-size changes in time. As for our previous analyses, we used the option in *dadi* to apply the folded SFS since we cannot polarize the SNPs and masked out singletons. For each model, we

calculated the maximum likelihood parameter estimates and computed the optimized likelihood. This likelihood was used to select the best fitting model by applying the Akaike information criterion (AIC). Second, we used *StairwayPlot2* using the default settings to estimate the single population demographic histories. *StairwayPlot2* has the advantage that no specific demographic scenario needs to be specified a priori and can estimate more complex demographic histories. As before, we used the folded SFS for the analyses. Since we did not know the exact number of nucleotides sites from which the 2019 SNPs were extracted from, we arbitrarily used 100000 sites, which means that age and population-size estimates need to be considered carefully. Additionally, we assumed a clock rate of 2.1E-9 (Keightley et al., 2014).

2.9 | Phylogenetic analysis of the 12 populations

We estimated the relationship between the 12 populations using two separate phylogenetic approaches. First, we applied the polymorphism-aware phylogenetic models (PoMos, [De Maio et al., 2013, 2015]) as implemented in the software RevBayes (Borges et al., 2022; Höhna et al., 2016). PoMos model allele frequency changes under a Moran process and provide a powerful approach to estimate population trees from polymorphic data such as SNP data. As PoMos are not yet available for time-calibration because the branch lengths of a PoMo analysis are in Moran units and scaled to the virtual population size, we estimated a relative time-tree without absolute time. Nevertheless, the phylogenetic relationship and ordering as well as relative distance of the population splitting events is informative for the colonialization process.

2.10 | Estimating the node to *P. pyralis*

To increase our understanding on the population history of *P. pyralis*, we estimated a time-calibrated phylogenetic tree. This time-calibrated phylogeny will provide an estimate of the divergence time of *P. pyralis* from its sister species and an upper limit estimate of the oldest population beyond the presently studied populations. We compiled a new dataset with 37 taxa from the *Photinus* clade. We performed a GenBank search using the taxon tag 'Photinus' through the software SUMAC (version 2.2.0) (Freyman, 2015). Sequences belonging to this taxonomic group were clustered in putative orthoclusters using the UCLUST algorithm (version 6.0.0) (Edgar, 2010). Orthoclusters were aligned with MAFFT (version 6.2.40) (Katoh et al., 2002) and badly aligned regions were removed using Gblocks (version 0.91b) (Talavera & Castresana, 2007). Sequence duplicates were removed and further alignment curation was done manually with AliView (version 1.18.1) (Larsson, 2014). After curation, seven orthoclusters representing seven genes were chosen for phylogenetic node calibration: *Cytochrome c oxidase subunit I* (COI, length: 1264 nt, sequences: 37), *28S ribosomal RNA* (28S, length: 365 nt, sequences: 7), *16S ribosomal RNA* (16S, length: 414 nt, sequences: 12), *18S ribosomal RNA* (28S, length: 681 nt, sequences: 12), *UV opsin* (UV, length: 1081 nt, sequences: 18), *wingless* (WG, length: 404 nt, sequences: 36) and *carbamoyl-phosphate synthetase 2* (CAD, length: 577 nt, sequences: 31). These genes have been used to diagnose species-level relationships in fireflies previously (Martin et al., 2017; Sander & Hall, 2015; Stanger-Hall et al., 2007; Stanger-Hall & Lloyd, 2015) (Appendix S1: I).

In this analysis, we applied a Bayesian relaxed-clock analysis with data partitioned by gene. Specifically, we assumed a GTR + Gamma + I substitution model (Tavaré, 1986) where among site rate variation was modelled by 4 discrete categories obtained from a gamma distribution (Yang, 1994) and an additional category for invariant sites independently for each gene. We applied default prior distributions for the substitution model parameters, that is a flat Dirichlet prior distributions on both the stationary frequencies and on the exchangeability rates (Höhna et al., 2017). Furthermore, to account for rate variation among lineages, we used a relaxed-clock model with uncorrelated lognormal distributed rates (UCLN) (Drummond et al., 2006). We applied an uninformative hyperprior distribution on both the mean ~ uniform(0, 100) and standard deviation, SD ~ uniform(0,100) of the branch-specific clock rates. We calibrated the phylogeny using a birth-death process as the prior on divergence times and a normal prior distribution with mean 42.5 and standard deviation of 2.5 on the root age. This age was obtained from Höhna et al. (2022).

We employed the following strategy to estimate the posterior distribution of phylogenies. We ran a four-replicate Metropolis-Coupled Markov chain Monte Carlo (MCMCMC) analysis with one cold chain and three heated chains, as implemented in RevBayes v. 1.0.12 (Höhna et al., 2016), for 50000 iterations and sampled phylogenetic trees and parameters states every 10 iterations, yielding a total of 20000 samples from the posterior distribution. We checked for convergence of our MCMC runs using the R package *convenience* (Fabreti & Höhna, 2022). The scripts used in the analyses described in the methods section can be found in https://doi.org/10.5281/zenodo.7018803.

3 | RESULTS

3.1 | Population clustering for demographic inference

We used published RADseq data generated for 154 individuals sampled from 12 populations across the United States, yielding a total of 308 sequenced chromosomes, to elucidate the demographic history of *P. pyralis* (Figure 1a) (Lower et al., 2018). We first examined evidence for grouping the populations into larger clusters, with the aim of reducing the number of possible demographic scenarios to test and to facilitate uncovering the mode of colonization of *P. pyralis*. We performed a DAPC (Jombart et al., 2010) analysis using a $k = 3$, to evaluate pooling the populations into three genetic clusters: a Texan cluster (including two Texan populations), a Central (Arkansas,

TABLE 1 Posterior probabilities of each multi-population demographic model

Population combinations	P(*M1*)	P(*M2*)	P(*M3*)	P(*M4*)	P(*M5*)	Power
Pooled populations	1	0	0	0	0	89.8%
DETX, DEMI, MANJ	0.9934	0	0	0	0.0065	82.6%
VATX, BYMS, ATGA	1	0	0	0	0	91.8%
VATX, SLMO, HFTN	0.9999	0	0	0.0001	0	75%

Note: The first row shows the model probabilities of the pooled genetic clusters in each area (Texas, Central and East). Rows two to four show the model probabilities when only one random population per area was chosen as representative. The mean power of model choice (last column) slightly decreases with the non-pooled data, but the overall support for *Model 1* remains.

Mississippi, Missouri, Ohio and Michigan) and an Eastern cluster (Georgia, Tennessee, North Carolina and New Jersey) (Table S1). Our DAPC analysis supported the three above-mentioned clusters with high membership probabilities (Appendix S1: II, Figure 1b). We thus decided to use these three population clusters for the demographic inference (Figure 1).

3.2 | Population genetics summary statistics

After data filtering (see Section 2.3), from the original 2019 SNPs for all populations combined, we kept 1196, 1381 and 1190 SNPs for the Texan, Central and Eastern clusters, respectively. For the genetic clusters, we observed an overall nucleotide diversity (as estimated by θ_W and π) of Texan > Central > Eastern, although nucleotide diversity values across the three genetic clusters were close from each other (Table S2). For single-population estimates of θ_W and π, Central > Texan > Eastern was the found pattern. The high nucleotide diversity found in the Central populations could be result of admixture, as depicted in a fastSTRUCTURE analysis, when evaluating values of $k = 2$ to $k = 7$ (Figure S2). When looking further at single populations, Tajima's *D* values were all positive, suggesting either population structure, balancing selection and/or population-size contractions. When pooling the populations, the increase in the number of segregating sites (which affects θ_W) was proportionally larger than the increase (if any) in the average number of pairwise nucleotide differences (which affects π), thus resulting in a reduction in Tajima's *D* for the pooled populations. Linkage disequilibrium was variable across single populations, but in general values showed low LD estimates. After pooling the populations, the levels of LD (as measured by Z_{nS}) increased due to the influx of new segregating sites (Table S2).

Next, we calculated the Wakeley–Hey W statistics in order to estimate the degree of isolation between populations by summarizing the joint site-frequency spectrum (JSFS). From this analysis, when looking at private and shared polymorphisms between populations (W1, W2 and W4), we found that the Central and Eastern clusters are the closest to one another, when compared to the Texan (Table S3). We also observed that there are almost no fixed differences between any pair of clusters and that most of the polymorphisms present in this dataset are either private or shared between each pair of populations (Table S3). Our single-population Wakeley–Hey W analysis closely resembled the genetic cluster approach (Tables S4–S6). This pattern was also congruent when calculating population differentiation as measured by F_{st}, where population differentiation correlates with geographic distance (Tables S3–S6).

3.3 | Model choice for ABC demographic inference

Validation of model choice using simulated datasets shows a high power (I- type_II_error) for selecting the right model among the four tested scenarios. More specifically, for the genetic clusters, *Models 1* through *5* are chosen correctly 95%, 87%, 84%, 90% and 93% of the time, respectively. For combinations of single populations, the power is reduced slightly due to having less data, but there was still enough power to validate our model-choice procedure. With this high validation power, we then proceeded to calculate the posterior probabilities of all four models given the observed data (Table 1). We found that *Model 1* (southern origin + sequential colonization) has the highest probability in both the pooled (99.9%) and non-pooled populations (90–100%, Table 1). *Model 1* is able to predict well all tested summary statistics, that is, in all cases, the observed summary statistic fell within the distribution of simulated statistics under *Model 1* (Figure S3).

3.4 | Parameter estimation

By using partial least squares (pls), we reduced the dimensionality of all summary statistics down to 10 pls components. This procedure is favourable since the new set of transformed statistics is orthogonal to each other, guaranteeing the assumption of singularity, which is required for ABC regression (Beaumont et al., 2002). Validation of parameter estimation showed good power to estimate all parameters, population sizes and timing of population splits, except for the selection coefficient S_{Aa} (Figure S4). All estimates (except for S_{Aa}) are given relative to Ne_{Texas}.

Overall, the data reflect that the Central cluster has an effective population size bigger to that of the Texan and that the Eastern is much smaller than the Texan cluster. This pattern changes when single populations are analysed; here, populations coming from the Central and Eastern cluster show a smaller population size when compared to either of the Texan populations (Tables S8–S10). The split between the Eastern and Central clusters happened around

Demographic models	Texan cluster	Central cluster	Eastern cluster
(1) Neutral equilibrium ($p = 1$)	683.24 (−340.62)	1082 (−540.38)	753.88 (−375.94)
(2) Two-epoch ($p = 3$)	**205.38 (−99.69)**	421.2 (−207.60)	**365.52 (−179.76)**
(3) Growth ($p = 3$)	205.68 (−99.84)	423.0 (−208.50)	366.00 (−180.00)
(4) Bottle-growth ($p = 5$)	209.38 (−99.69)	425.2 (−207.6)	370.00 (−180.00)
(5) Three-epoch ($p = 5$)	209.38 (−99.69)	**420.24 (−205.12)**	369.22 (−179.61)

TABLE 2 AIC scores and log-likelihoods of five demographic scenarios tested by *dadi*

Note: For each population, bold indicates the demographic model with the lowest AIC and thus the best fitting model. The AIC score is presented first and the log-likelihood in parenthesis. The number of parameters *p* is given for each model.

$0.0048^{*}4Ne_{Texas}$ generations ago (Table S7, Figure S5) and the split between the Central and the Texan happened $0.026^{*}4Ne_{Texas}$ generations ago. Even though these time estimates vary in the single-population analysis, the Central population always show a colonization time older of that of the Eastern populations (Tables S8–S10). Finally, alternative models with migration between populations have also been analysed but there was not enough power to tell migration from no-migration models (Table S11).

3.5 | Dadi and StairwayPlo2 analyses

To further investigate demographic processes shaping nucleotide diversity, we used *dadi* (Gutenkunst et al., 2009) to test for five specific demographic scenarios (see Methods) and the *StairwayPlot2* method, in order to detect past changes in population size (Liu & Fu, 2020). In the *dadi* analysis, the demographic scenario that had the lowest likelihood for the three genetic clusters was the constant population-size scenario, clearly indicating that the three genetic clusters have gone through population changes. For all three clusters, the demographic scenarios depicting population-size changes had a very close fit (Table 2, Figure S6). This pattern was consistent when testing the 12 individual populations (Figure S7).

The best fitting scenario for the Texan cluster was the two-epoch scenario, suggesting that this cluster underwent a population shrinkage 0.00026 $2N_e$ generations ago (Table S12). For the Central cluster, the three-epoch scenario had the best fit, going first through a population expansion and then through a population shrinkage. The two-epoch model was also the best fit for the Eastern population, depicting a population shrinkage 0.01566 $2N_e$ generations ago (Table S12).

In the *StairwayPlot2* analysis, the three genetic clusters and the single-population data showed a similar pattern (Figure S8), where most of the populations showed a fairly constant population size back in time, with a gradual population decline towards the present. From this pattern, two exceptions were observed in the Eastern cluster and in the SMLO population, where a bottleneck was detected.

3.6 | Population-level phylogenetic tree estimation

Using a phylogenetic tree approach to study genetic relationships among populations can provide additional information for demographic inference hypothesis testing. We thus performed a PoMo analysis. Because PoMo uses virtual population sizes within the Moran process, the phylogenetic relationships cannot be scaled for actual times, at the moment (Borges et al., 2022). Nevertheless, branch lengths do represent proportional genetic differentiation across populations. The posterior probability of the topology shown in Figure 2 was approximately 1.0, which gives us high confidence that the three represent the genetic relationships of the tested populations.

3.7 | Estimating the upper limit of the age of the most ancient population of *P. pyralis*

To increase our understanding on the population history of *P. pyralis*, we estimated the age of its phylogenetic node. The age of the node to *P. pyralis* gives us an estimate of the upper limit of the maximum age for its most ancient population as well as the geological time scale of when this event happed. We obtained a time-calibrated phylogeny from a Bayesian relaxed-clock analysis of the *Photinus* & *Ellychnia* clade using seven loci (16S, 18S, 28S, CAD, COI, UV opsin and WG). The relationships in the phylogeny agree with prior publications using parts of the same gene (see e.g. [Sander & Hall, 2015; Stanger-Hall & Lloyd, 2015]). From this phylogeny, we estimated the age of the node between *P. pyralis* and its sister species *P. concisus* to be 5.96 [4.03–8.17] Ma old (Figure 3). This result suggests that the age of the most ancient population of *P. pyralis* is ~6 Ma or younger, which corresponds to the end of the Miocene epoch.

4 | DISCUSSION

4.1 | Demographic inference of *P. pyralis*

To start uncovering the demographic history of *P. pyralis*, we analysed several populations sampled in North America (Lower et al., 2018) (Figure 1a). Our approach consisted in using different existing methods for demographic inference (*ABC* demographic analysis, *dadi*, *PoMo*) and population history events (*StariwayPlot2*) to have a better understanding of the demographic process that happened in the past. From the five demographic hypotheses that we tested using *AB* (Figure 1C), *Model 1* had the highest probability when compared with

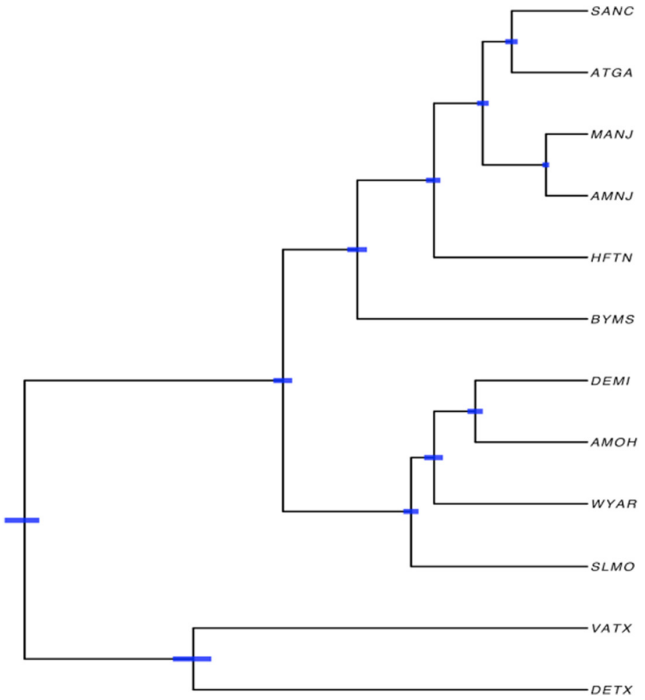

FIGURE 2 Population-level phylogenetic analysis as implemented in PoMo of 12 *P. pyralis* populations. Blue horizontal bars represent 95% credible intervals of relative time of divergence

the rest of the models, when testing the genetic clusters and the randomly chosen single populations. *Model 1* described a scenario where the Texan population was the first to colonize North America. The Central population is derived from the Texan one and in turn, the Eastern population is derived from the Central population. This stepwise colonization process, as depicted in *Model 1*, showed a 99.9% probability when compared to the four remaining models. Our study confidently rejects a demographic scenario in which colonization happened the other way around, from the Eastern US to Texas (*Model 2*). The demographic scenarios where the Central and the Eastern populations were independently colonized from Texas (*Model 3*) or where the Central population is the most ancestral one (*Model 4*) had zero model support. *Model 5* was also rejected, a model where we explored a non-sequential colonization process which could be plausible in the presence of refugial pockets left from a pre-ice age panmictic population. A stepwise colonization pattern has been reported for the North American eastern subterranean termite (*Reticulitermes flavipes*), where southern populations expanded their distribution range northward the Appalachian mountains (Hyseni & Garrick, 2019), exemplifying that a stepwise colonization, might have been the mode of dispersion for some insects.

The levels of LD (as measured by Z_{nS}) vary between populations, and in this case, the Texan had the highest LD, followed by the Eastern, and finally the Central cluster with the lowest LD (Table S2). The strength of LD can increase due to gene flow between populations (especially when allele frequencies differ among populations), when recombination rates are low or after a recent migration event (Slatkin, 2008). Changes in population size can also influence LD levels, such as bottlenecks which could potentially increase LD levels due to the loss of alleles (Zhang et al., 2004). Finally, positive selection is also a factor that can lead to an increase in LD as a consequence of genetic hitchhiking during a selective sweep (Kim & Stephan, 2002).

When looking at the Wakeley–Hey W and Fst statistics, we observe a gradient in terms of shared polymorphisms, where the number of shared polymorphisms decreases with geographic distance (Table S3–S6), a result that agrees with a demographic scenario where a stepwise colonization has taken place. Additionally, the fact that 32–43% of the SNPs are shared across populations and the low number of fixed differences between all populations, suggest that the colonization of the Central and the Eastern populations are more recent events. Alternatively, high levels of shared polymorphisms across populations can also be obtained under the presence of gene flow (Wakeley & Hey, 1997). The wide distribution of *P. pyralis* already suggests its high dispersion capacity, thus making the presence of gene flow between populations plausible. Consequently, we also tested models including migration, but with our current RADseq data, there was not enough power to distinguish between migration from no-migration models (Table S11). Migration models would benefit significantly by obtaining more SNPs and haplotypes sampled from whole genomes.

The population-specific statistics, Tajima's *D*, LD (as measured by Z_{nS}), and the joint SFS, already suggest that each population might have undergone size changes. Consequently, by using *dadi* and a *StairwayPlot2* analysis, we found that the populations have undergone size changes. The general pattern observed from these analyses, at the genetic cluster and single-population level, is the detection of a population decline pattern (Figure S8–S9, Table S12). In the *dadi* analysis, the two-epoch model had the highest probability for the Texan and the Eastern clusters, where a population decline is described (Table S12). The three-epoch model fitted best the Central population, showing that this population went through a population expansion followed by a shrinkage (Table S12). The relative time of the population decline obtained with *dadi* showed a stepwise pattern, where the decline occurs first in the Texan cluster and then in the Central and lastly in the Eastern cluster. This result complements well our *ABC* analysis on a stepwise colonization from Texans to the Northeast of the United States. Nevertheless, given the close fit of all the models tested with *dadi* (Table 2, Figure S7), the above proposed demographic scenarios will benefit from further testing.

From the *StairwayPlot2* analysis, we uncovered the signal of a bottleneck in the Eastern cluster and in the population from St. Louis, Missouri (Figures S8–S9). The hypothesis of a bottleneck occurring in some of the populations mark the possibility that some populations have managed to recover after a population decline. Demographic events can be very dynamic in nature, especially with constant climate changes and changes in habitat availability. As natural habitats usually tend to shrink due to human impact, it is not surprising that we found a signal of population shrinkage in most populations that goes up to the Quaternary (Figures S8–S9). For some of the populations, the intense luciferase harvesting from

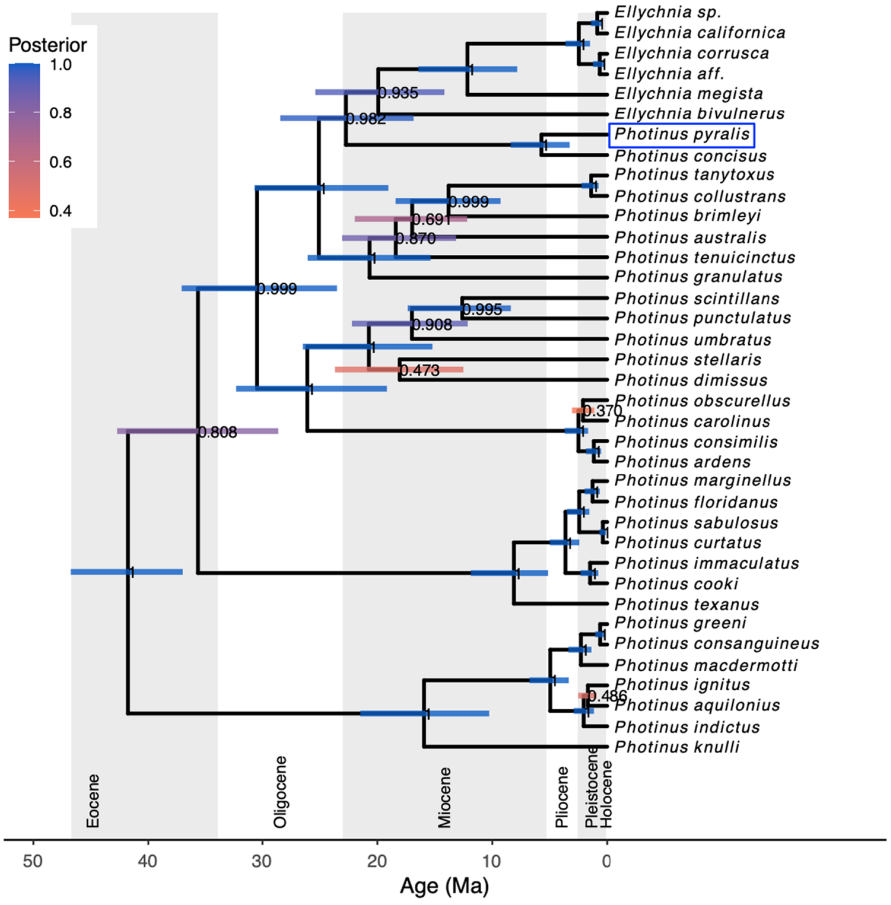

FIGURE 3 Phylogenetic tree indicating the node ages in million years (MA) for the *Photinus* group (*Photinus* and *Ellychnia*) plotted using the R package RevGadgets (Tribble et al., 2022). Horizontal bars at the nodes indicate 95% credible intervals of node ages. Legend indicates posterior probabilities of the node ages. Blue square highlights *P. pyralis*

natural populations (Bauer et al., 2013) could have been an additional cause of population decline.

From our demographic modelling, the size of the Central cluster is slightly larger (~1.43 times larger) than that of the Texan population. The Central cluster has the highest number of segregating sites and the lowest values of LD when compared to the other populations, which hints to high connectivity across the single populations or shared ancestral polymorphism (Table S7). Nevertheless, when single populations are analysed, Texas always shows the biggest population size (Tables S8–S10). In the case of the Eastern cluster, it shows a population size 0.0020 smaller than that of the Texan population (Figure S5, Table S7). The relatively small Eastern population size can be a result of a recent colonization event, putatively a post-glaciation event, or higher selective pressures that do not allow for bigger population sizes (e.g. winter). The small population size of the Eastern cluster was also supported by *dadi*, which supported a more recent population shrinkage. The low and homogeneous genetic diversity of the Eastern population (Tables S2, S3) could also have been maintained by isolation through the Appalachian mountain ranges, serving as a geographic barrier between the Eastern populations and both, the Central and Texan populations, as found in other North American taxa (Soltis et al., 2006).

We further estimated the relative time of colonization of the Central and Eastern clusters in relation to the Texan effective population size. Nevertheless, because we do not have the actual estimate of the Texan population size, we can only express time estimates relative to the effective population size *Ne* of the Texan population. The *Ne* in other insects, for example *Drosophila melanogaster* (Arguello et al., 2019) and *Heliconius melpomene* (Keightley et al., 2015), has been estimated to be around 2 million individuals for both species. If the *Ne* of *P. pyralis* is also close to 2 million individuals; then, we can infer that the Central population was founded ~400000 years ago, and the Eastern ~75000 years ago. Following this time estimate, ~400000 years ago was a warm interglacial period during the Pleistocene which could have been leveraged by *P. pyralis* to colonize new habitats, settling populations in the Center of the United States (Mississippi, Arkansans, Illinois) (Raynaud et al., 2005). Consequently, ~75000 years ago was also an interglacial period (Grimley et al., 2003), which would have facilitated the settlement of populations in the East coast of the United States. We hypothesize that the Pleistocene glaciations (~2.58 MYA to the present) had the most impact on North American *P. pyralis*'s current geographical distribution. Some of the locations where our populations were collected (e.g., New Jersey and Michigan), were covered by ice during the last glaciation (Bemmels & Dick, 2018), making these areas habitable only after a glacial retreat. The future estimation of effective population sizes in *P. pyralis* will help us to more accurately infer the colonization times of the Central and Eastern populations as well as to better understand the role of glacial refugia in *P. pyralis*' current distribution.

Two variables will help to get a more accurate estimate of the colonization time. The first one will be estimating the mutation rate

of *P. pyralis*, which is not a trivial task, but plausible by either generating pedigree lines or by generating population-level whole-genome data from which we can draw mutation rate estimates by using synonymous sites (Yang & Nielsen, 1998), microsatellites (Whittaker et al., 2003) or pseudogene variation (Nachman & Crowell, 2000). The second factor influencing the estimation of the time of colonization is the generation time of *P. pyralis*, which is hypothesized to vary across populations. For example, the populations inhabiting northern latitudes such as the Eastern population only produce one generation every 2 years, whereas southern populations are hypothesized to produce two generations a year (Fallon et al., 2018; Faust, 2017). More research on the life cycle of *P. pyralis* will help to get more precise values of the generation time, which we can then include in our demographic models.

Our population-based phylogenetic analysis done by PoMo confidently supports a scenario where the Texan populations are the most diverged from the Central and Eastern populations. The topology shown in Figure 2 confidently rejects a scenario where fragmentation of an ancestral continuous population took place as a result of an ice age (*Model5*), as in such a scenario, we would expect most of the populations to originate from the same population, resulting in a star-like tree topology. Instead, we observe that the Texan populations are differentiated from the Central and Eastern populations. The tree in Figure 2 might suggest a scenario similar to *Model 3*, where the Central and the Eastern clusters were derived independently from the Texan cluster. Nevertheless, *Model 3* does not have statistical support (Table 1). The population phylogenetic trees do support a stepwise colonization process from Texas to the East, although we acknowledge that the populations forming the Central cluster might have undergone alternative demographic histories.

Finally, we estimated the age of the node to *P. pyralis* as an approximation of the upper limit of the maximum age for the species origin. This age would mark the age of the most ancient population of *P. pyralis*, which could have arisen in much southern latitudes than the Texan populations that we sampled. From our time-calibration study (Figure 3), we estimated the age of the node representing the split between *P. pyralis* and *P. concisus* to be ~6 million years. The occurrence of *P. pyralis* in Mexico, Central and South America together with the estimated divergence age to *P. concisus* raises the question of where does *P. pyralis* most ancestral population originated and sets a limit on the geological events influencing its distribution. Additionally, the fact that the most ancestral population of *P. pyralis* is 6 million years old, opens the possibility that its presence in North America is a geologically recent colonization.

5 | CONCLUSIONS

Our study on the demographic history of *P. pyralis* has generated the first demographic hypothesis for North American populations. The plausible stepwise colonization route taken by *P. pyralis*, from Texas to New Jersey, possibly taking advantage of interglacial periods, is an example of patterns of insect colonization of North America from natural populations. This research fills the gap in the current literature, which focuses mainly on invasive or economically important species. Moreover, the estimation of the node leading to *P. pyralis* sets the age, end of the Miocene, of its most ancestral population and opens up the question of where this population originated. Finally, inferring the demographic history of *P. pyralis* also provides a neutral reference for nucleotide diversity patterns, which we can use to assess deviations caused by natural selection, which will help us understand the adaptive events that lead to the wide distribution of this firefly.

ACKNOWLEDGEMENTS

We would like to acknowledge our funding the DFG, CA2207/3-1, HO6201/1-1, HO6201/2-1.

CONFLICT OF INTEREST

The authors declare no conflicts of interest.

PEER REVIEW

The peer review history for this article is available at https://publons.com/publon/10.1111/jeb.14094.

DATA AVAILABILITY STATEMENT

The data that support the findings of this study are available in https://doi.org/10.5281/zenodo.7018803

ORCID

Ana Catalan https://orcid.org/0000-0002-4543-748X
Sebastian Höhna https://orcid.org/0000-0001-6519-6292
Pablo Duchen https://orcid.org/0000-0002-9318-5002

REFERENCES

Arguello, J. R., Laurent, S., & Clark, A. G. (2019). Demographic history of the human commensal Drosophila melanogaster. *Genome Biology and Evolution*, *13*, 844–854.

Arias, O., Cordeiro, E., Corrêa, A. S., Domingues, F. A., Guidolin, A. S., & Omoto, C. (2019). Population genetic structure and demographic history of Spodoptera frugiperda (Lepidoptera: Noctuidae): Implications for insect resistance management programs. *Pest Management Science*, *75*, 2948–2957.

Bauer, C. M., Nachman, G., Lewis, S. M., Faust, L. F., & Reed, J. M. (2013). Modeling effects of harvest on firefly population persistence. *Ecological Modelling*, *256*, 43–52.

Beaumont, M. A., Zhang, W., & Balding, D. J. (2002). Approximate Bayesian computation in population genetics. *Genetics*, *162*, 2015–2035.

Bemmels, J. B., & Dick, C. W. (2018). Genomic evidence of a widespread southern distribution during the last glacial maximum for two eastern north American hickory species. *Journal of Biogeography*, *45*, 1739–1750.

Borges, R., Boussau, B., Szöllősi, G. J., & Kosiol, C. (2022). Nucleotide usage biases distort inferences of the species tree. *Genome Biology and Evolution*, *14*, 1–13.

Cione, A. L., Gasparini, G. M., Soibelzon, E., Soibelzon, L. H., & Tonni, E. P. (2015). *The great American biotic interchange: A south American perspective*. Springer US.

Cock, R. D., & Matthysen, E. (1999). Aposematism and Bioluminescence: Experimental evidence from Glow-worm Larvae(Coleoptera: Lampyridae). *Evolutionary Ecology*, *13*, 619–639. https://doi.org/10.1023/A:1011090017949

Csilléry, K., François, O., & Blum, M. G. B. (2012). Abc: An R package for approximate Bayesian computation (ABC). *Methods in Ecology and Evolution*, *3*, 475–479.

De Maio, N., Schlötterer, C., & Kosiol, C. (2013). Linking great apes genome evolution across time scales using polymorphism-aware phylogenetic models. *Molecular Biology and Evolution*, *30*, 2249–2262.

De Maio, N., Schrempf, D., & Kosiol, C. (2015). PoMo: An allele frequency-based approach for species tree estimation. *Systematic Biology*, *64*, 1018–1031.

Drummond, A. J., Ho, S. Y. W., Phillips, M. J., & Rambaut, A. (2006). Relaxed phylogenetics and dating with confidence. *PLoS Biology*, *4*, 699–710.

Duchen, P., Zivkovic, D., Hutter, S., Stephan, W., & Laurent, S. (2013). Demographic inference reveals African and European admixture in the north American *Drosophila melanogaster* population. *Genetics*, *193*, 291–301.

Edgar, R. C. (2010). Search and clustering orders of magnitude faster than BLAST. *Bioinformatics*, *26*, 2460–2461.

Ewing, G., & Hermisson, J. (2010). MSMS: A coalescent simulation program including recombination, demographic structure and selection at a single locus. *Bioinformatics*, *26*, 2064–2065.

Excoffier, L., Dupanloup, I., Huerta-Sánchez, E., Sousa, V. C., & Foll, M. (2013). Robust demographic inference from genomic and SNP data. *PLoS Genetics*, *9*, e1003905.

Fabreti, L. G., & Höhna, S. (2022). Convergence assessment for Bayesian phylogenetic analysis using MCMC simulation. *Methods in Ecology and Evolution*, *13*, 77–90.

Fallon, T. R., Lower, S. E., Chang, C.-H., Bessho-Uehara, M., Martin, G. J., Bewick, A. J., Behringer, M., Debat, H. J., Wong, I., Day, J. C., Suvorov, A., Silva, C. J., Stanger-Hall, K. F., Hall, D. W., Schmitz, R. J., Nelson, D. R., Lewis, S. M., Shigenobu, S., Bybee, S. M., … Weng, J.-K. (2018). Firefly genomes illuminate parallel origins of bioluminescence in beetles. *eLife*, *7*, 1–146.

Faust L. F. (2017). *Fireflies, glow-worms, and lightning bugs: Identification and natural history of the fireflies of the eastern and central United States and Canada*. University of Georgia Press.

Freyman, W. A. (2015). SUMAC: Constructing phylogenetic supermatrices and assessing partially decisive taxon coverage. *Evolutionary Bioinformatics*, *11*, 263–266.

Grimley, D. A., Follmer, L. R., Hughes, R. E., & Solheid, P. A. (2003). Modern, Sangamon and Yarmouth soil development in loess of unglaciated southwestern Illinois. *Quaternary Science Reviews*, *22*, 225–244.

Gutenkunst, R. N., Hernandez, R. D., Williamson, S. H., & Bustamante, C. D. (2009). Inferring the joint demographic history of multiple populations from multidimensional SNP frequency data. *PLoS Genetics*, *5*, e1000695.

Havill, N. P., Shiyake, S., Lamb, G. A., Foottit, R. G., Yu, G., Paradis, A., Elkinton, J., Montgomery, M. E., Sano, M., & Caccone, A. (2016). Ancient and modern colonization of North America by hemlock woolly adelgid, Adelges tsugae (Hemiptera: Adelgidae), an invasive insect from East Asia. *Molecular Ecology*, *25*, 2065–2080.

Hewitt, G. M. (2004). Genetic consequences of climatic oscillations in the quaternary. *Philosophical Transactions of the Royal Society B: Biological Sciences*, *359*, 183–195.

Höhna, S., Landis, M. J., & Heath, T. A. (2017). Phylogenetic inference using RevBayes. *Current Protocols in Bioinformatics*, *2017*, 6.16.1–6.16.34.

Höhna, S., Landis, M. J., Heath, T. A., Boussau, B., Lartillot, N., Moore, B. R., Huelsenbeck, J. P., & Ronquist, F. (2016). RevBayes: Bayesian phylogenetic inference using graphical models and an interactive model-specification language. *Systematic Biology*, *65*, 726–736.

Höhna, S., Lower, S. E., Duchen, P., & Catalán, A. (2021). A Time-calibrated Firefly (Coleoptera: Lampyridae) Phylogeny: Using Genomic Data for Divergence Time Estimation. *bioRxiv*. https://doi.org/10.1101/2021.11.19.469195

Hyseni, C., & Garrick, R. C. (2019). The role of glacial-interglacial climate change in shaping the genetic structure of eastern subterranean termites in the southern Appalachian Mountains, USA. *Ecology and Evolution*, *9*, 4621–4636.

Jaskuła, R., Kolanowska, M., Michalski, M., & Schwerk, A. (2021). From phenology and habitat preferences to climate change: Importance of citizen science in studying insect ecology in the continental scale with american red flat bark beetle, cucujus clavipes, as a model species. *Insects*, *12*, 1–22.

Jombart, T., & Ahmed, I. I. (2011). Adegenet 1.3-1: New tools for the analysis of genome-wide SNP data. *Bioinformatics*, *27*, 3070–3071.

Jombart, T., Devillard, S., & Balloux, F. (2010). Discriminant analysis of principal components: A new methods for the analysis of genetically structured populations. *BMC Genetics*, *11*, 1–15.

Katoh, K., Misawa, K., Kuma, K., & Miyata, T. (2002). MAFFT: A novel method for rapid multiple sequence alignment based on fast Fourier transform. *Nucleic Acids Research*, *30*, 3059–3066.

Keightley, P. D., Ness, R. W., Halligan, D. L., & Haddrill, P. R. (2014). Estimation of the spontaneous mutation rate per nucleotide site in a Drosophila melanogaster full-sib family. *Genetics*, *196*, 313–320.

Keightley, P. D., Pinharanda, A., Ness, R. W., Simpson, F., Dasmahapatra, K. K., Mallet, J., Davey, J. W., & Jiggins, C. D. (2015). Estimation of the spontaneous mutation rate in *Heliconius melpomene*. *Molecular Biology and Evolution*, *32*, 239–243.

Kelly, J. K. (1997). A test of neutrality based on interlocus associations. *Genetics*, *146*, 1197–1206.

Kim, Y., & Stephan, W. (2002). Detecting a local signature of genetic hitchhiking along a recombining chromosome. *Genetics*, *160*, 765–777.

Lait, L. A., & Hebert, P. D. N. (2018). Phylogeographic structure in three north American tent caterpillar species (Lepidoptera: Lasiocampidae): *Malacosoma americana*, *M. californica*, and *M. disstria*. *PeerJ*, *2018*, 1–23.

Larsson, A. (2014). AliView: A fast and lightweight alignment viewer and editor for large datasets. *Bioinformatics*, *30*, 3276–3278.

Lewis, S. M., & Cratsley, C. K. (2008). Flash signal evolution, mate choice, and predation in fireflies. *Annual Review of Entomology*, *53*, 293–321.

Liu, X., & Fu, Y. X. (2020). Stairway plot 2: Demographic history inference with folded SNP frequency spectra. *Genome Biology*, *21*, 1–9.

Lloyd, J. E. (1966). *Studies on the flash communication system in Photinus fireflies* (Vol. *130*, pp. 1–95). Miscellaneous Publications. Museum of Zoology, University of Michigan.

Lloyd, J. E. (1975). Aggressive Mimicry in Photuris Fireflies: Signal Repertoires by Femmes Fatales. *Science*, *187*, 452–453.

Lower, S. E., Stanger-hall, K. F., & Hall, D. W. (2018). Molecular variation across populations of a widespread north American firefly, Photinus pyralis, reveals that coding changes do not underlie flash color variation or associated visual sensitivity. *BMC Evolutionary Biology*, *18*, 1–14.

Mann, P. (2007). Overview of the tectonic history of northern CentralAmerica. *Geological Society of America Special Papers*, *428*, 1–19.

Martin, G. J., Branham, M. A., Whiting, M. F., & Bybee, S. M. (2017). Total evidence phylogeny and the evolution of adult bioluminescence in fireflies (Coleoptera: Lampyridae). *Molecular Phylogenetics and Evolution*, *107*, 564–575.

Myers, E. A., McKelvy, A. D., & Burbrink, F. T. (2020). Biogeographic barriers, Pleistocene refugia, and climatic gradients in the southeastern Nearctic drive diversification in cornsnakes (*Pantherophis guttatus* complex). *Molecular Ecology*, *29*, 797–811.

Nachman, M. W., & Crowell, S. L. (2000). Estimate of the mutation rate per nucleotide in humans. *Genetics*, *156*, 297–304.

Nei, M., & Li, W. H. (1979). Mathematical model for studying genetic variation in terms of restriction endonucleases. *Proceedings of the National Academy of Sciences of the United States of America*, *76*, 5269–5273.

Papadopoulou, A., & Knowles, L. L. (2015). Genomic tests of the species-pump hypothesis: Recent Island connectivity cycles drive population divergence but not speciation in Caribbean crickets across the Virgin Islands. *Evolution*, *69*, 1501–1517.

Pritchard, J. K., Seielstad, M. T., & Feldman, M. W. (1999). Population growth of human Y chromosomes: A study of Y chromosome microsatellites. *Molecular Biology and Evolution*, *16*, 1791–1798.

Raj, A., Stephens, M., & Pritchard, J. K. (2014). FastSTRUCTURE: Variational inference of population structure in large SNP data sets. *Genetics*, *197*, 573–589.

Raynaud, D., Barnola, J.-M., Souchez, R., Lorraint, R., Petit, J.-R., Duval, P., & Lipenkov, V. Y. (2005). The record for marine isotopic stage 11. *Nature*, *436*, 39–40.

Roy, A. J., & Lachniet, M. S. (2010). Late quaternary glaciation and equilibrium-line altitudes of the Mayan ice cap, Guatemala, Central America. *Quaternary Research*, *74*, 1–7.

Sander, S. E., & Hall, D. W. (2015). Variation in opsin genes correlates with signalling ecology in north American fireflies. *Molecular Ecology*, *24*, 4679–4696.

Slatkin, M. (2008). Linkage disequilibrium - understanding the evolutionary past and mapping the medical future. *Nature Reviews. Genetics*, *9*, 477–485.

Soltis, D. E., Morris, A. B., McLachlan, J. S., Manos, P. S., & Soltis, P. S. (2006). Comparative phylogeography of unglaciated eastern North America. *Molecular Ecology*, *15*, 4261–4293.

Stanger-Hall, K. F., & Lloyd, J. E. (2015). Flash signal evolution in *Photinus fireflies*: Character displacement and signal exploitation in a visual communication system. *Evolution*, *69*, 666–682.

Stanger-Hall, K. F., Lloyd, J. E., & Hillis, D. M. (2007). Phylogeny of north American fireflies (Coleoptera: Lampyridae): Implications for the evolution of light signals. *Molecular Phylogenetics and Evolution*, *45*, 33–49.

Tajima, F. (1989). Statistical method for testing the neutral mutation hypothesis by DNA polymorphism. *Genetics*, *595*, 585–595.

Talavera, G., & Castresana, J. (2007). Improvement of phylogenies after removing divergent and ambiguously aligned blocks from protein sequence alignments. *Systematic Biology*, *56*, 564–577.

Tavaré, S. (1986). Some probabilistic and statistical problems in the analysis of DNA sequences. *American Mathematical Society. Lectures on Mathematics Life Science*, *17*, 57–86.

Tavare, S., Balding, D. J., Griffiths, J. R. C., & Donnelly, P. (1997). Inferring coalescence TimesFrom DNA sequence. *Genetics*, *145*, 505–518.

Vencl, F. V., & Carlson, A. D. (1998). Proximate mechanisms of sexual selection in the firefly *Photinus pyralis* (Coleoptera : Lampyridae). *Journal of Insect Behavior*, *11*, 191–207.

Wakeley, J., & Hey, J. (1997). Estimating ancetral population parameters. *Genetics*, *145*, 847–855.

Watterson, G. A. (1975). On the number of segregating sites in genetical models without recombination. *Theoretical Population Biology*, *276*, 256–276.

Wegmann, D., Leuenberger, C., & Excoffier, L. (2009). Efficient approximate Bayesian computation coupled with Markov chain Monte Carlo without likelihood. *Genetics*, *182*, 1207–1218.

Weir, B. S., & Cockerham, C. C. (1984). Estimating F-statistics for the analysis of population structure. *Evolution*, *38*, 1358–1370.

Whittaker, J. C., Harbord, R. M., Boxall, N., Mackay, I., Dawson, G., & Sibly, R. M. (2003). Likelihood-based estimation of microsatellite mutation rates. *Genetics*, *164*, 781–787.

Yang, Z. (1994). Maximum likelihood phylogenetic estimation from DNA sequences with variable rates over sites: Approximate methods. *Journal of Molecular Evolution*, *39*, 306–314.

Yang, Z., & Nielsen, R. (1998). Synonymous and nonsynonymous rate variation in nuclear genes of mammals. *Journal of Molecular Evolution*, *46*, 409–418.

Zhang, W., Collins, A., Gibson, J., Tapper, W. J., Hunt, S., Deloukas, P., Bentley, D. R., & Morton, N. E. (2004). Impact of population structure, effective bottleneck time, and allele frequency on linkage disequilibrium maps. *Proceedings of the National Academy of Sciences*, *101*, 18075–18080.

SUPPORTING INFORMATION

Additional supporting information can be found online in the Supporting Information section at the end of this article.

How to cite this article: Catalan, A., Höhna, S., Lower, S. E., & Duchen, P. (2022). Inferring the demographic history of the North American firefly *Photinus pyralis*. *Journal of Evolutionary Biology*, *35*, 1488–1499. https://doi.org/10.1111/jeb.14094